Academic Article

Summer Heatstroke Risk Prediction for Tokyo in the 2030s Based on Mesoscale Simulations by WRF

Masataka Kasai*[1]   Tsubasa Okaze*[2]   Miguel Yamamoto*[1]   Akashi Mochida*[1]   Kazumasa Hanaoka*[3]

*[1] Department of Architecture and Building Science, Graduate School of Engineering, Tohoku University
*[2] School of Environment and Society Department, Architecture and Building Engineering, Tokyo Institute of Technology
*[3] Department of Geography, College of Letters, Ritsumeikan University

Corresponding author: Masataka KASAI, kasai@sabine.pln.archi.tohoku.ac.jp

ABSTRACT

This study aims to quantify the spatial distribution of summertime outdoor heatstroke risk in the Tokyo metropolitan area of Japan. Heatstroke risk was quantified by assessing the overlap of hazard, vulnerability, and exposure. As the hazard index, the daily maximum wet-bulb globe temperature (WBGT) was selected. To predict the spatial distribution of the WBGT at urban scale, mesoscale meteorological simulations using Weather Research and Forecasting (WRF) model were performed. The actual daily incidence rate of heatstroke, which was assumed to be a function of the observed daily maximum WBGT, was estimated as the vulnerability index. The monthly incidence rate was obtained using the hazard and vulnerability indices. Finally, the total number of heatstroke patients per month could be estimated as a heatstroke risk index by multiplying the monthly incidence rate by the population density. To understand the impact of climate change on the heatstroke risk, the current (2000s) and near future (2030s) risk distributions were estimated by applying the proposed method. The risk increased by more than 20% at coastal regions in the 2030s, owing to changing climate conditions such as increase in humidity.

Key Words : Heatstroke risk, WBGT, Incidence rate, Future prediction, Tokyo metropolitan area, WRF

1. Introduction

During the summer of 2010, Japan experienced a serious heat wave in which the number of heatstroke patients transported by ambulance in Tokyo rose to approximately ten times that of previous years[1]. Since 2010, the number of heatstroke patients has remained at elevated values. The Intergovernmental Panel on Climate Change (IPCC)[2] has concluded that continued warming of 0.3 °C to 4.8 °C by the end of the 21st century is probable. Therefore, an evaluation of heatstroke risk under future climate conditions is required in order to take the appropriate countermeasures.

The working group on future standard weather prediction using global climate model (GCM) at the Architectural Institute of Japan has developed a method to construct standard weather data used to calculate the building thermal load[3]-[4]. The working group used data from the Model for Interdisciplinary Research on Climate version 4 (MIROC4h)[5], which is one of the GCMs, as the initial and boundary conditions for a regional climate model (RCM). The Weather Research and Forecasting

(WRF) model was used as the RCM, and MIROC4h data was physically downscaled using the WRF. Using the WRF simulation results, the standard weather data for the future (2030s) were constructed for major cities in Japan such as Tokyo, Osaka, Nagoya, and Sendai.

On the other hand, several previous studies have estimated the mesoscale heatstroke risk. Ohashi et al.[6] used the daily maximum wet-bulb globe temperature (WBGT) as an index of the outdoor heat stress and estimated the number of heatstroke patients as the heatstroke risk in Tokyo in 2010. Kikumoto et al.[7] estimated the incidence rates of heatstroke both in the current and near future in the Tokyo metropolitan area. However, the effect of the population distribution was not considered, and the absolute number of heatstroke patients was not discussed. Recently, the authors[8] developed a method to estimate the absolute number of outdoor heatstroke patients as the heatstroke risk, and validated the method for the summer of 2010 in Sendai, Japan.

To understand the impact of climate change on heatstroke risk, this study aims to predict the distribution of the outdoor

incidence rate of heatstroke and the number of outdoor heatstroke patients both currently (2000s) and in the near future (2030s) in August in the Tokyo metropolitan area of Japan, based on mesoscale meteorological simulations with WRF.

2．Method for estimation of heatstroke risk

Figure 1 illustrates the conceptual model for disaster risk evaluation[9]. In the field of disaster prevention, the risk of each disaster is largest for locations where hazard, vulnerability, and exposure intersect. Hazard represents dangerous factors that cause natural disasters. Vulnerability represents potential weaknesses that increase the disaster risk for a region. Exposure represents the number of people or amount of time spent exposed to the hazard, and is generally quantified by the population in the region.

In this study, risk was defined as the number of outdoor heatstroke patients transported by ambulance for a given location and time period. The three indices of hazard, vulnerability, and exposure were defined as the daily maximum WBGT, the relationship between the daily maximum WBGT and the daily incidence rate, and the daytime population density, respectively.

The outdoor WBGT is generally calculated from Eq. (1)[10]:

$$WBGT = 0.1Ta + 0.7Tw + 0.2Tg \tag{1}$$

where Ta is the dry-bulb temperature [°C], Tw is the wet-bulb temperature [°C], and Tg is the globe temperature [°C]. In this study, the distributions of the hourly WBGT were estimated using several meteorological factors simulated by WRF. The details of the WRF simulations are described in Chapter 3. Although Ta was equal to the air temperatures obtained directly from the WRF simulations, Tw and Tg were estimated from several WRF outputs, respectively. Tw was estimated using air temperature, absolute humidity, and atmospheric pressure[11]-[12]. Tg was estimated from Eq. (2)[13]:

$$Tg = \begin{cases} Ta + 12.1 + 0.0067S - 2.40v^{1/2} & (S > 400 \text{ W/m}^2) \\ Ta - 0.3 + 0.0256S - 0.18v^{1/2} & (S \le 400 \text{ W/m}^2) \end{cases} \tag{2}$$

where S is the global solar radiation [W/m²] and v is the wind velocity [m/s]. The solar radiation to the ground surface and horizontal wind velocitiy at 10-m were obtained from the WRF simulations and used for S and v in Eq. (2), respectively. Finally, the daily maximum WBGT was obtained from the hourly estimates and used as the hazard index for heatstroke risk evaluation.

To define the vulnerability index, the relationship between the observed daily maximum WBGT value and the actual recorded number of heatstroke patients transported by ambulance in Tokyo's 23 wards was analyzed. The emergency transport data included the transport dates and places where heatstroke occurred for each heatstroke patient recorded from May to

September in 2010 and 2011. We extracted only outdoor cases from the transport data to estimate the vulnerability index in this study. On the other hand, we estimated the daily maximum WBGT using hourly-observed meteorological data near the Tokyo station (Otemachi) by the Tokyo District Meteorological Observatory, Japan Meteorological Agency. Previous studies[6]-[7] used observational data from Otemachi to reveal the relationship between the WBGT and incidence rate in Tokyo. We followed these and used meteorological data from the same observatory. Using this data, the relationship between the daily maximum WBGT and daily incidence rate of outdoor heatstroke patients transported by ambulance per 1,000,000 people per day (IR_{day} [persons/(1,000,000 population·day)]) was obtained.
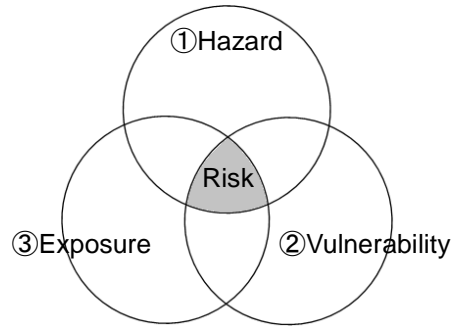

Fig. 1: Concept for disaster risk[9]
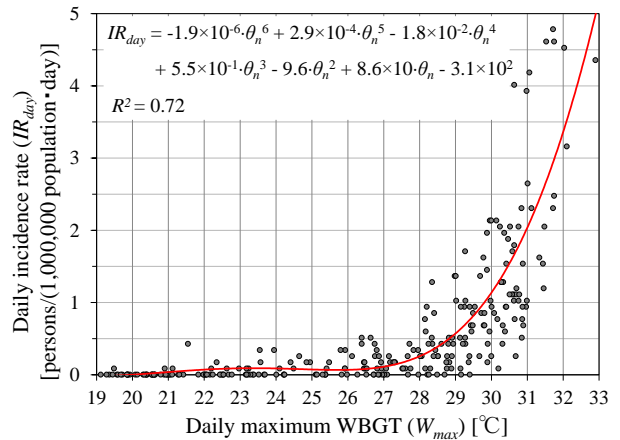
Fig. 2: Relationship between the daily maximum WBGT and IR_{day}
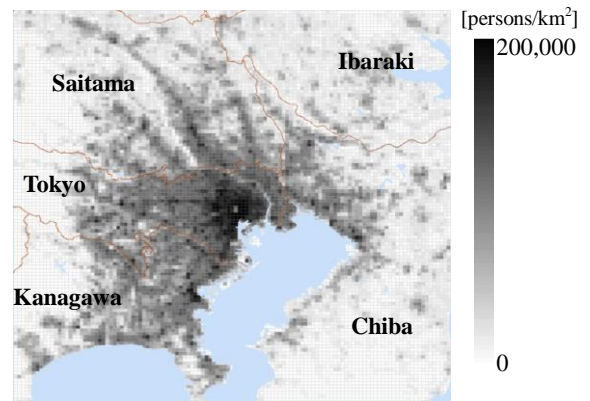
Fig. 3: Daytime population density in the Tokyo metropolitan area

Figure 2 illustrates the IR_{day} for Tokyo as a function of the daily maximum WBGT. Figure 3 illustrates the spatial distribution of the daytime population density per 1 km^2 in the Tokyo metropolitan area, based on the Population Census of 2010[14] and the Economic Census of 2009[15], which was used as the exposure index of the risk evaluation. To analyze exclusively the impact of climate change on heatstroke risk in the future, it was assumed that the population density would remain the same. Using the three indices representing hazard, vulnerability, and exposure, heatstroke risk is estimated as shown below:

$$IR_{day} = -1.9 \times 10^{-6} \cdot W_{max}{}^6 + 2.9 \times 10^{-4} \cdot W_{max}{}^5$$
$$- 1.8 \times 10^{-2} \cdot W_{max}{}^4 + 5.5 \times 10^{-1} \cdot W_{max}{}^3$$
$$- 9.6 \cdot W_{max}{}^2 + 8.6 \times 10 \cdot W_{max} - 3.1 \times 10^2 \quad (3)$$

$$IR_{month} = \sum_{day=1}^{max} IR_{day} \quad (4)$$

$$Risk = (IR_{month} \times PD)/10^6 \quad (5)$$

where W_{max} is the daily maximum WBGT. Equation (3) gives the polynomial approximations for the IR_{day} of Tokyo as a function of daily maximum WBGT, as seen in Fig. 2. The determination coefficient (R^2 value) of Eq. (3) was 0.72. By summing IR_{day} during one month, the monthly incidence rate (IR_{month} [persons/(1,000,000 population·month)]) was calculated (Eq. (4)). Finally, by substituting IR_{month} and the daytime population density (PD [persons/km^2]) in Eq. (5), the absolute number of heatstroke patients transported by ambulance (*Risk* [persons/(km^2·month)]) was estimated. The accuracy of the method has been validated by comparing the predicted number of heatstroke patients in Sendai of 2010 with the actual recorded number of patients[8].

3．**Mesoscale meteorological simulations with WRF**

3.1 **Outline of simulations**

Mesoscale meteorological simulations with WRF were performed to obtain distributions of the daily maximum WBGT for use as the hazard index. The calculation results of a GCM named MIROC4h[5], which followed the RCP4.5 scenario[16], was selected as the global scale meteorological data. Since the horizontal resolution of MIROC4h data is approximately 60 km × 60 km, we could not analyze the details of the thermal environment at the urban scale. Hence, we conducted simulations with a finer grid resolution by WRF using MIROC4h data for the initial and boundary conditions, to predict climate conditions at the urban scale. Figure 4 shows the computational domains for WRF and the land use distribution in the smallest domain, namely Domain 3. We focused on the Tokyo metropolitan area. The calculation conditions and physics schemes used in the WRF simulations are summarized in Tables 1 and 2, respectively. The horizontal resolution of Domain 3 was 1 km × 1 km. We selected representative summers for WRF

simulations in the 2000s and 2030s based on the monthly average air temperature in August by MIROC4h. During the period from 2006 to 2010, specifically in 2007, the monthly average temperature in the Tokyo metropolitan area was closest to the regression line of the observed value from 1981 to 2010. Thus, we selected the summer of 2007 as the representative summer in the current situation. Further, we selected the summer of 2031, in which the monthly average temperature was approximately 1 °C higher than that in 2007 as the representative summer of the near future situation. We ran WRF simulations for both summers from July 15 to September 1. The first two weeks were used for spin-up.

3.2 **Comparison of results for meteorological simulations in 2000s and 2030s**

From the WRF simulations, the meteorological factors needed for calculating the WBGT could be obtained. Figure 5 illustrates the spatial distributions for differences in the monthly average
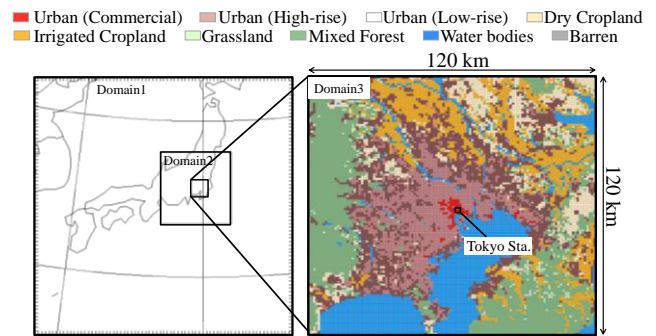

Fig. 4: Domains for WRF simulationsand land use map of Domain 3

Table 1: Calculation conditions for WRF simulations

Date	21:00 (JST) Jul. 15 ~ 21:00 (JST) Sept. 1
Grid Arrangement	Dom. 1: 72 × 72 (Grid size: 25 km) Dom. 2: 150 × 150 (Grid size: 5 km) Dom. 3: 120 × 120 (Grid size: 1 km)
Time Interval	Dom. 1: 90 s, Dom. 2: 30 s, Dom. 3: 6 s
Number of Vertical Grids	34 (from the surface to the 50 hPa level)
Topographic Data	Doms. 1, 2: U.S. geological survey Dom. 3: Japanese national land numerical information[17]
Nesting	One-way nesting

Table 2: Physics schemes for WRF simulations

Microphysics	WRF single-moment 6-class scheme
Shortwave Radiation	Dudhia scheme
Longwave Radiation	Rapid radiative transfer model scheme
Land Surface	Noah land surface model + Single-layer urban canopy model
Planetary Boundary Layer	Yonsei University scheme
Cumulus Parameterization	Kain-fritsch (new Eta) scheme

(1) air temperature and (2) absolute humidity at a height of 2-m and time of 12:00 p.m. between 2007 and 2031. The monthly average inland air temperatures at noon in the future were higher than 31 °C even though that of the coastal area was relatively low, owing to the cooling effect of the sea breeze. However, the increase of temperature from 2007 to 2031 in the coastal area was larger than that of inland area as seen in Fig. 5 (1). Since there were a few more cloudy days in 2031 than in 2007, the solar radiation to the ground surface in 2031 was less than that in 2007. Therefore, the air temperature in 2031 in the northwest part of the center of Tokyo changed little compared with that in 2007. According to the results of MIROC4h, the monthly

average sea surface temperature used as the boundary condition of WRF near Tokyo in 2031 increased 1.6 °C compared with that in 2007, while the increase in monthly average land surface temperature was only 0.3 °C. This increase in sea surface temperature led to the increase in air temperature on the sea.

The humidity along the coastal areas was higher than that of the mountainous areas in the western part of the area studied. Moreover, the discrepancy in humidity between the coastal area and inland area further widened in the future (2031). This was probably caused by the increase of evaporation from sea surface and the advection of humidity resulting from the sea breeze.

Because of the difficulty to set the detailed distribution of the

(1) Air temperature

(2) Absolute humidity
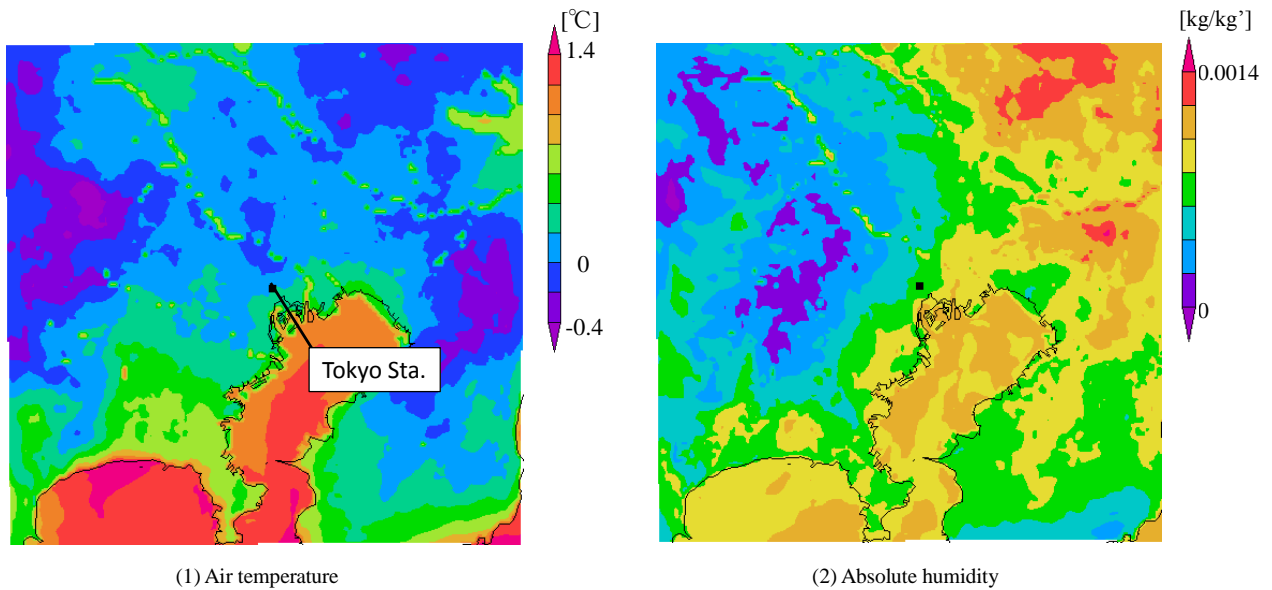
Fig. 5: Differences in monthly average meteorological factors at 12:00 (2031－2007)
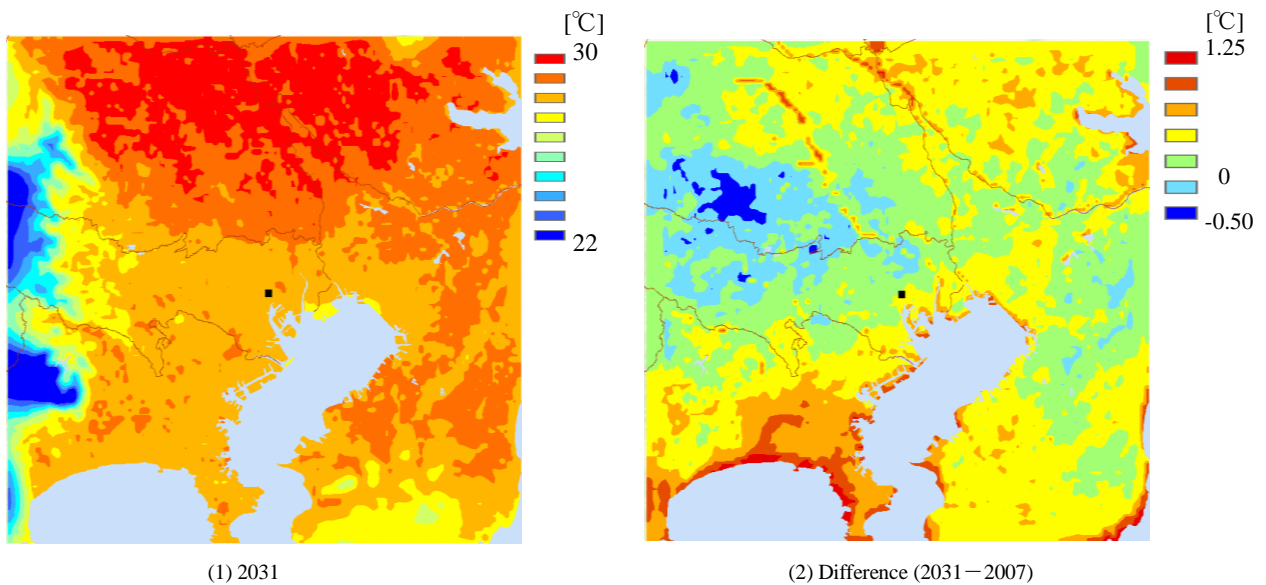
(1) 2031

(2) Difference (2031－2007)

Fig. 6: Monthly average daily maximum WBGT

[persons/(1,000,000 population·month)]

[persons/(1,000,000 population·month)]

(1) 2031

(2) Difference (2031－2007)

Fig. 7: Monthly incidence rate (*IR_month*)

[persons/(km²·month)]

[persons/(km²·month)]

(1) 2031

(2) Difference (2031－2007)
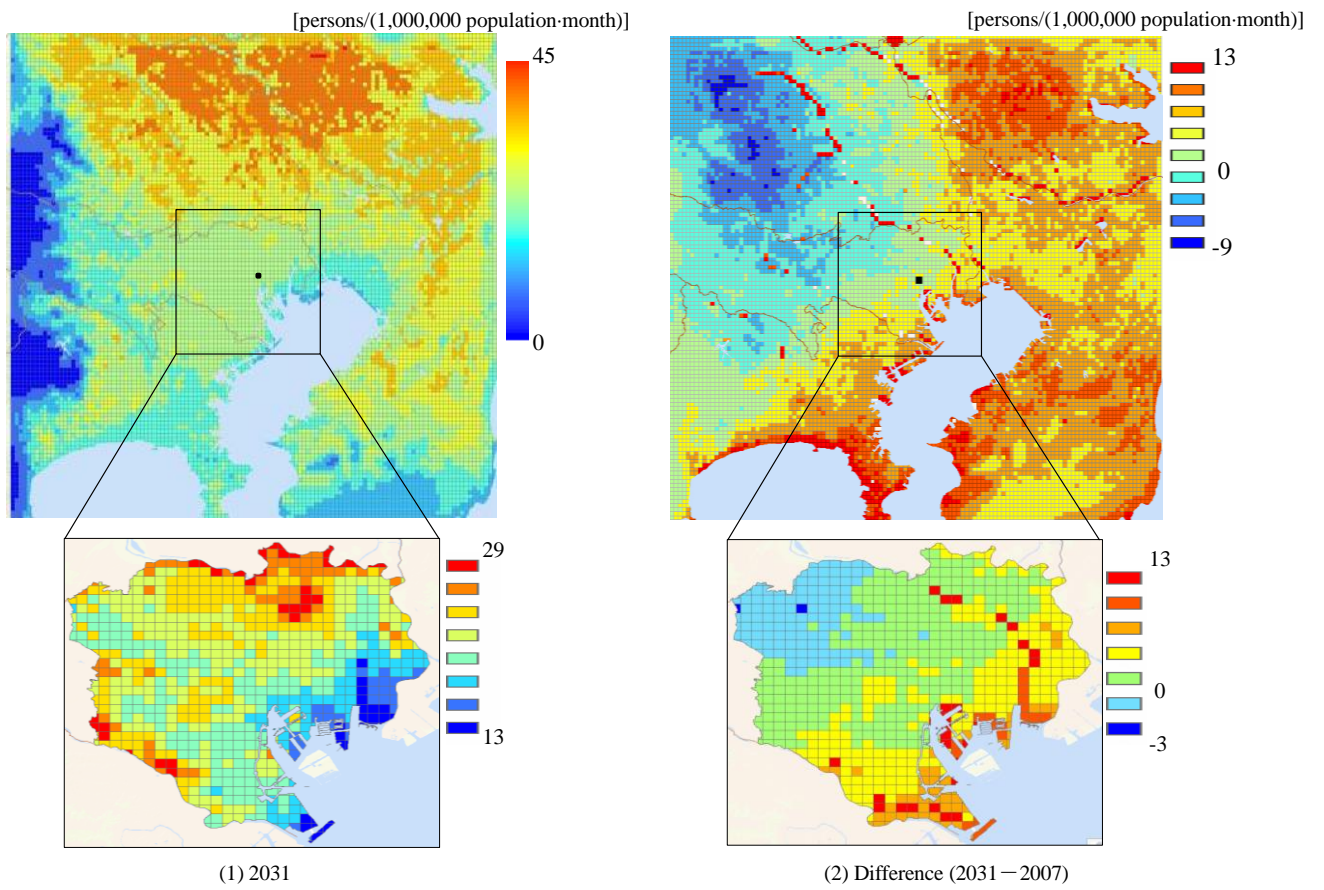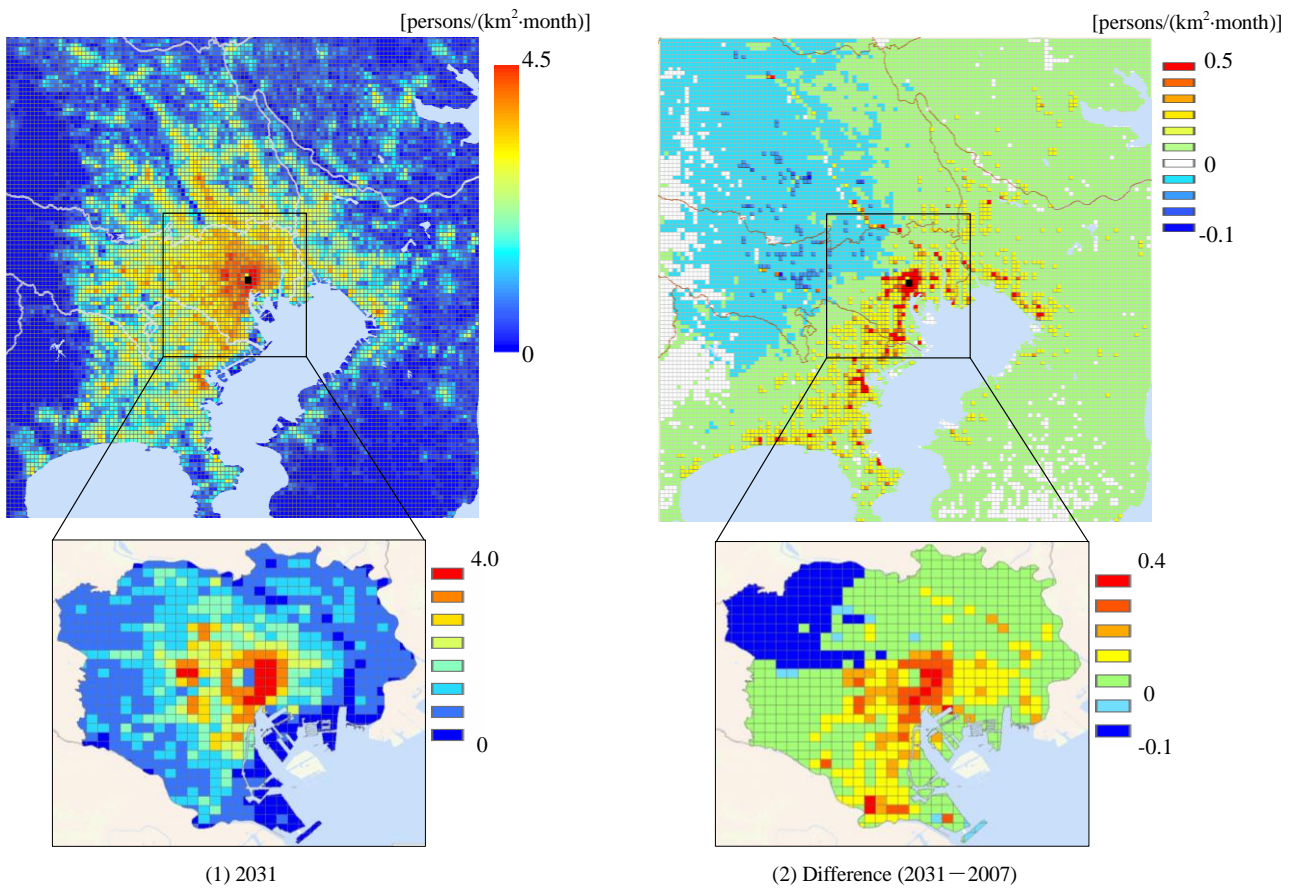
Fig. 8: The number of heatstroke patients (*Risk*)

river surface temperature in the Tokyo metropolitan area from the results of GCM, the river surface temperature for the WRF simulations was given by assuming the same as the sea surface temperature near the river in this study. Therefore, increasing of air temperature and humidity along the rivers appeared similar to that on the sea. Figure 6 shows the spatial distributions for (1) the monthly average daily maximum WBGT in 2031 and (2) the difference between 2031 and 2007 (2031−2007) calculated using the method outlined in Chapter 2. Since the weight coefficient of the wet-bulb temperature is largest in the equation for calculating WBGT (Eq. (1)), the WBGT increased by approximately 0.5 °C for the future at the area with the largest increase in humidity. Hence, the hazard for the heatstroke risk will increase significantly in coastal areas including Tokyo and Yokohama, which are some of the most densely populated regions in Japan.

4．Estimation of outdoor incidence rate and heatstroke risk

Applying the proposed method mentioned in Chapter 2 to the WBGT distributions obtained from the WRF simulations, the outdoor incidence rate per month (IR_{month}) and the number of heatstroke patients ($Risk$) in the Tokyo metropolitan area can be estimated. Figure 7 illustrates (1) the IR_{month} in 2031, and (2) the difference in IR_{month} between 2031 and 2007 (2031−2007). The IR_{month} at the northern inland area was approximately twice as high as that of the coastal area. However, the tendency of the increased IR_{month} was significant at the waterfront because of the high-WBGT change from 2007 to 2031 caused by the increase in humidity. This indicated that risk would become obvious in the future at coastal areas where the regional potential risk is not as high under the current climate conditions.

Considering the population density as the exposure index, $Risk$ can be estimated. Figure 8 illustrates (1) the $Risk$ in 2031 and (2) difference in $Risk$ between 2031 and 2007 (2031−2007). The total predicted number of heatstroke patients in Tokyo was approximately 370 people in August 2031. Figure 8 (2) shows that the expansion of the $Risk$ was concentrated at the coastal areas, such as the central part of Tokyo. This resulted from the synergistic effects of an increase in humidity with global warming and a high population density. Figures 7 and 8 additionally show the detailed distributions in Domain 3, focusing on Tokyo's 23 wards. Ohashi et al.[6] carried out a pioneering work where the incidence rate and the heatstroke risk in Tokyo's 23 wards under actual summer conditions in 2010 were estimated. They showed that the incidence rate in the western inland part of the 23 wards in 2010 was higher than in the coastal part, and that the absolute number of heatstroke patients was concentrated in the center of Tokyo's 23 wards.

Although we estimated the outdoor heatstroke risk in the future, the distributions of IR_{month} and $Risk$ qualitatively corresponded with the study by Ohashi et al[6].

The results of this study show that the increased rate in $Risk$ of each prefecture in the Tokyo metropolitan area from 2007 to 2031 was proportional to the length of the coastline (Chiba: 23.8%, Kanagawa: 21.8%, Tokyo: 5.2%, Saitama: -1.6%)

5．Conclusions

Outdoor incidence rate and risk of heatstroke in the 2000s and 2030s for the Tokyo metropolitan area were estimated using the results from mesoscale meteorological simulations with WRF.

The risk evaluation was based on the concept that disaster can occur when hazard, vulnerability, and exposure intersect. The results of this study suggest that the hazard for heatstroke risk, the daily maximum WBGT, will increase mainly along coastal areas in the future, owing to a large increase in humidity with global warming. The IR_{month} at northern inland area was found to be twice that of the coastal area, including the central part of Tokyo in 2030s. This means that the regional potential risk was very high in the inland area. However, the tendency for the increased IR_{month} was more significant along coastal areas in the future (2030s). Finally, the $Risk$ increased by more than 20% at coastal regions in the 2030s.

References

(1) National Institute for Environmental Studies Bulletin Report on Heatstroke Patients, 2015 Bulletin Report on Heatstroke Patients, https://www.nies.go.jp/health/HeatStroke/spot/2015/tokyo.pdf

(2) Intergovernmental Panel on Climate Change, Contribution of Working Group I to the Fifth Assessment Report of the IPCC, Climate Change 2013: The Physical Science Basis

(2013).

(3) R. Ooka, et al., The near future weather data for building energy simulation using dynamical downscaling of results from global climate model, AIJ Journal of Technology and Design, 20-46 (2014), pp.325-359.

(4) Y. Arima, et al., Effect of climate change on building cooling loads in Tokyo in the summers of the 2030s using dynamically downscaled GCM data, Energy and Buildings, 114 (2016), pp.123-129.

(5) T. Sakamoto, et al., Miroc4h-A New High-Resolution Atmosphere-Ocean Coupled General Circulation Model, Journal of Meteorological Society of Japan, 90-3 (2012), pp. 325-359.

(6) Y. Ohashi, et al., Numerical simulations of outdoor heat stress index and heat disorder risk in the 23 wards of Tokyo, Journal of Applied Meteorology and Climatology, 53 (2014), pp. 583-597.

(7) H. Kikumoto, R. Ooka, Y. Arima, A study of urban thermal environment in Tokyo in summer of the 2030s under influence of global warming, Energy and Buildings, 114 (2016), pp. 54-61.

(8) M. Kasai, et al., Prediction of heatstroke risk in Sendai in summer of 2030s based on mesoscale simulation by WRF, Proceedings of The Fifth International Conference on Human-Environment System (2016).

(9) Intergovernmental Panel on Climate Change, Contribution of Working Group II to the Fifth Assessment Report of the IPCC, Climate Change 2014: Impacts, Adaptation, and Vulnerability (2014).

(10) C.P. Yaglou, D. Minard, Control of heat casualties at military training centers, A.M.A. Archives of Industrial Health, 16-4 (1957), pp. 302-316.

(11) O. Tetens, Uber einige meteorologische Begriffe, Zeitschrift fur Geophysik, 6 (1930), pp. 297-309.

(12) J. V. Iribarne, W. L. Godson, Atmospheric Thermodynamics, (1981), D. Reidel Publishing Company.

(13) M. Tonouchi, K. Murayama, Regional characteristics for the risk of heatstroke and HWDI, Japanese Journal of Biometeorology, 45-3 (2008), S62.

(14) Ministry of Internal Affairs and Communications, Results of National Census (2010), http://www.stat.go.jp/data/index.htm.

(15) Ministry of Internal Affairs and Communications, Results of Economic Census (2009), http://www.stat.go.jp/data/index.htm.

(16) Richard H. Moss, et al, The next generation of scenarios for climate change research and assessment, Nature, 463-7283 (2010), 747-756.

(17) Ministry of Land, Infrastructure, Transport and Tourism, National Land Numerical Information (Land use subdivision mesh data), http://nlftp.mlit.go.jp/ksj/.